International Journal of Thermophysics, Vol. 22, No. 5, September 2001 (© 2001)

Emissivity Measurements and Modeling of Silicon-Related Materials: An Overview[1]

N. M. Ravindra,[2,3] B. Sopori,[4] O. H. Gokce,[2] S. X. Cheng,[2] A. Shenoy,[2] L. Jin,[2] S. Abedrabbo[2,5] W. Chen,[2,4,6] and Y. Zhang[2,4]

An overview of the emissivity measurements and modeling of silicon-related materials is presented. The experimental component of this investigation is based on results obtained utilizing spectral emissometry. An analysis of the comparison of the measured data with other similar approaches is made. In particular, the celebrated work of Sato is revisited to understand the implications of his study. Simulations of the temperature and wavelength dependent emissivity of silicon based on the semiempirical MULTIRAD model are presented. The influence of doping concentration, surface roughness, and coatings on the emissivity of silicon, as a function of temperature, is discussed.

KEY WORDS: coatings; concentration; doping concentration; emissivity; silicon; surface roughness; temperature; wavelength.

1. INTRODUCTION

Pyrometers are the instruments of choice for noncontact in situ temperature measurements in silicon processing. Pyrometers measure the amount of radiation emitted from a wafer within a narrow wavelength window. The ratio of the wafer emitted radiation to that of a blackbody under the

---

[1] Paper presented at the Fourteenth Symposium on Thermophysical Properties, June 25–30, 2000, Boulder, Colorado, U.S.A.

[2] New Jersey Institute of Technology, Department of Physics, 161 Warren Street, Newark, New Jersey 07102, U.S.A.

[3] To whom correspondence should be addressed. E-mail: nmravindra@home.com

[4] National Renewable Energy Laboratory, 1617 Cole Boulevard, Golden, Colorado 80401-3393, U.S.A.

[5] JDS Uniphase Corporation, 100 Willowbrook Road, Freehold, New Jersey 07728-2879, U.S.A.

[6] BTA Technology, 1982A Zanker Road, San Jose, California 95112, U.S.A.

0195-928X/01/0900-1593/0 © 2001 Plenum Publishing Corporation

same conditions of temperature, wavelength, angle of incidence, and direction of polarization is referred to as emissivity. Emissivity of silicon is a complicated function of both temperature and wavelength. In addition, it also varies with silicon dopant type, dopant concentration, surface roughness, and over/buried layers.

In the present study, the emissivity of silicon has been investigated. Comparisons of the experimentally measured emissivity have been made with the most celebrated work of Sato [1]. Simulations of the wavelength- and temperature-dependent emissivity of silicon, as functions of doping concentration and overlayers, using MULTIRAD [2] are presented.

2. EMISSIVITY FUNDAMENTALS

Emissivity is an important parameter in radiation thermometry. It is defined as the ratio of the radiance of a given object to that of a blackbody at the same temperature and for the same spectral and directional conditions. It is a function of wavelength and temperature. It is a property, which must be known for accurate temperature determination of an object by measurement of its emitted electromagnetic radiation with a radiation thermometer. The concept of emissivity and its correlation with other optical properties have been discussed earlier [1, 3, 4]. For completeness, these relations are revisited here. For normal incidence, the emissivity $\varepsilon(\lambda)$ of a plane-parallel specimen is given by

$$\varepsilon(\lambda) = [1 - R(\lambda)][1 - T(\lambda)]/[1 - R(\lambda)\, T(\lambda)] \tag{1}$$

where λ is the wavelength, $R(\lambda)$ is the true reflectance, and $T(\lambda)$ is the true transmittance. $R(\lambda)$ and $T(\lambda)$ are related to the fundamental optical parameters—$n(\lambda)$, the refractive index, and $k(\lambda)$, the extinction coefficient—by the following relations:

$$R(\lambda) = [\{n(\lambda) - 1\}^2 + k(\lambda)^2]/[\{n(\lambda) + 1\}^2 + k(\lambda)^2] \tag{2}$$

$$T(\lambda) = \exp[-\alpha(\lambda)\, t] = \exp[-4\pi k(\lambda)\, t/\lambda] \tag{3}$$

$\alpha(\lambda)$ is the absorption coefficient and t is the thickness of the material. Thus, from Eq. (1), for a perfect opaque body, since $T(\lambda) = 0$, Kirchoff's law follows as

$$\varepsilon(\lambda) = [1 - R(\lambda)] \tag{4}$$

The experimentally measured values of transmittance and reflectance include effects such as light trapping and multiple internal reflections

depending on the angle of incidence, surface roughness, presence of grains, grain boundaries, interface roughness, etc. The apparent transmittance $T(\lambda)^*$ and apparent reflectance $R(\lambda)^*$ are related to the real or true transmittance $T(\lambda)$ and true reflectance $R(\lambda)$, respectively, by the following well-known equations [4]:

$$T(\lambda)^* = T(\lambda)\,\frac{(1-R(\lambda))^2}{(1-R(\lambda)^2\,T(\lambda)^2)} \tag{5}$$

$$R(\lambda)^* = R(\lambda)\left\{1+\frac{T(\lambda)^2\,(1-R(\lambda))^2}{1-R(\lambda)^2\,T(\lambda)^2}\right\} \tag{6}$$

Equations (5) and (6) are the result of considering multiple internal reflections. Simultaneous measurement of reflectance and transmittance of double-side (optically) polished materials can yield true values of reflectance and transmittance and, therefore, the absorption coefficient, $\alpha(\lambda)$, the refractive index, $n(\lambda)$, and the extinction coefficient, $k(\lambda)$ of single substrate materials. With the choice of appropriate models, the $n(\lambda)$ and $k(\lambda)$ of multilayers can also be resolved from experimentally measured spectral properties.

3. EXPERIMENTAL

The schematic of the spectral emissometer is presented in Fig. 1. The detailed operation of this instrument has been discussed earlier [3, 6]. It consists of a hemiellipsoidal mirror providing two foci, one for the exciting source, in the form of a diffuse radiating near-blackbody source, and the other for the sample under investigation. A microprocessor-controlled motorized chopper facilitates simultaneous measurement of sample spectral properties such as radiance, reflectance, and transmittance. A carefully adjusted set of five mirrors provides the optical path for measurement of the optical properties. An oxyacetylene/propane torch provides the source of heating of the samples. The spectral emissometer utilizes the Helmholtz reciprocity principle [7] as explained in a related study [8].

4. RESULTS AND DISCUSSION

4.1. Temperature Measurement

The spectral emissometer allows for simultaneous measurements of the radiance R, reflectance ρ, transmittance τ, and temperature T of the

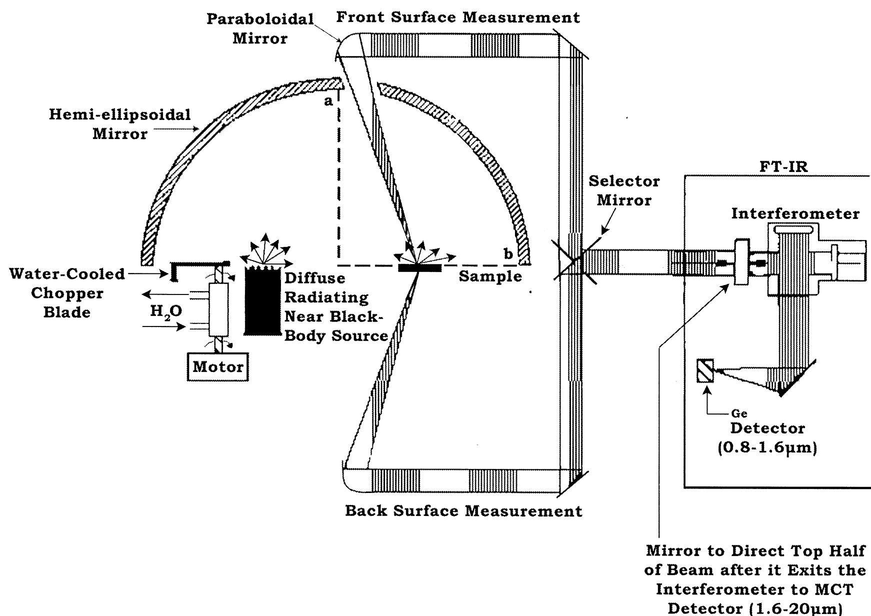

Fig. 1. Schematic of benchtop emissometer.

sample at the measured point. The theoretical background and methodology are as follows [9]. A sample is placed at one of the foci of the hemispherical ellipsoidal mirror, while the source, a blackbody at 900°C, is at the other foci. The chopper (in Fig. 1) permits the simultaneous acquisition of the radiative properties of interest including the sample temperature. A front-surface sample measurement, with the chopper closed, yields the sample's directional spectral radiance:

$$R_v(T) = \varepsilon_v(T)\, R_v{}^{\mathrm{b}}(T) \tag{7}$$

where $\varepsilon_v(T)$ is the emissivity of the sample at temperature T, and $R_v{}^{\mathrm{b}}$ is the theoretical Planck function at temperature T. The subscript v denotes the spectral frequency.

When the chopper is open, the measured radiation M_0 will include that emitted by the sample and the blackbody source radiation reflected by the sample in the spectral directional–hemispherical mode,

$$M_0 = R_v(T) + \rho_v(T)\, R_v{}^{\mathrm{b}}(T_{\mathrm{bb}}) \tag{8}$$

where T_{bb} is the constant blackbody source temperature, which is maintained at 900°C, and ρ_ν is the spectral directional–hemispherical reflectance. The difference in the two measurements is thus $\rho_\nu(T)\, R_\nu{}^b(T_{bb})$. The constant source radiation $R_\nu{}^b(T_{bb})$ is quantified by replacing the sample with a perfect reflector (a gold mirror, $\rho_{\nu,\,\mathrm{gold}} \approx 1.0$) and measuring the spectrum in the chopper open condition. Thus, the directional–hemispherical reflectance of the sample, $\rho_\nu(T)$, can be determined.

For an opaque sample, the spectral emittance $\varepsilon_\nu = 1 - \rho_\nu$. By rearrangement of Eq. (1), $R_\nu{}^b(T) = R_\nu(T)/\varepsilon_\nu(T)$, the surface temperature of the sample can be determined by direct integration over the whole spectral region,

$$\int R_\nu{}^b(T)\, d\nu = \sigma T^4 \tag{9}$$

The Stefan–Boltzmann constant $\sigma = 5.67 \times 10^{-12}\ \mathrm{W \cdot cm^{-2} \cdot K^{-4}}$. The sample temperature can be obtained to within ± 10°C. For nonopaque samples, the directional–hemispherical transmittance, τ_ν, is measured by flipping the selector mirror and measuring the back surface radiance and back surface radiance plus transmittance. The source radiation is quantified with the sample absent, and the analysis to determine τ_ν follows that for ρ_ν. The more extensive closure relationship, $\varepsilon_\nu = 1 - \rho_\nu - \tau_\nu$, is then used to determine ε_ν. The temperature of the samples can also be determined simultaneously by fitting the sample's radiance to the Plank's blackbody curves.

4.2. Results of Sato

Sato [1] has performed detailed work on the emissivity of silicon, in the wavelength range 0.4 to 15 μm and temperature range 340 to 1070 K. His paper has been a very valuable source of information for application of radiation pyrometry to silicon processing. However, to be able to compare the numerical values presented in Sato's work with similar studies, it is imperative that some corrections need to be applied to the scale in the horizontal wavelength axis in Figs. 3, 4, and 7 of Ref. 1. Basically, this has to do with replacing 20 for 15 μm in Figs. 3, 4, and 7 and replotting the data to reflect Sato's measurements in the wavelength range 0.5 to 15 μm. Also, the 0.5 μm, on the wavelength axis, has to be moved closer to the origin in Fig. 3. To accomplish this, we have digitized this figure. The results of this correction are presented in Fig. 2. This figure represents the experimental results of emissivity measurements of Sato. The sample considered in this study is an n-type, phosphorous-doped silicon of resistivity

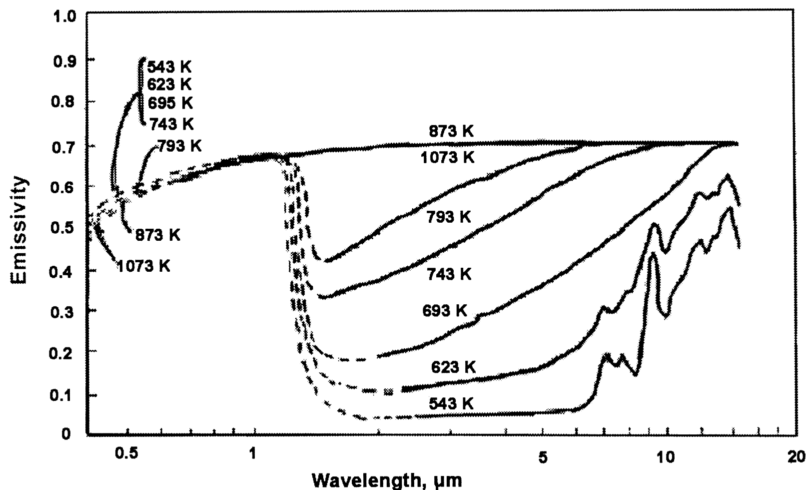

Fig. 2. Sato's [1] spectral emissivity of n-Si of thickness 1770 μm and doping concentration 2.94×10^{14} cm^{-3}. Solid curves: direct measurement. Dotted curves: indirect measurement—suggested modification to the wavelength axis (wavelength axis terminates at 20 μm instead of the original 15 μm).

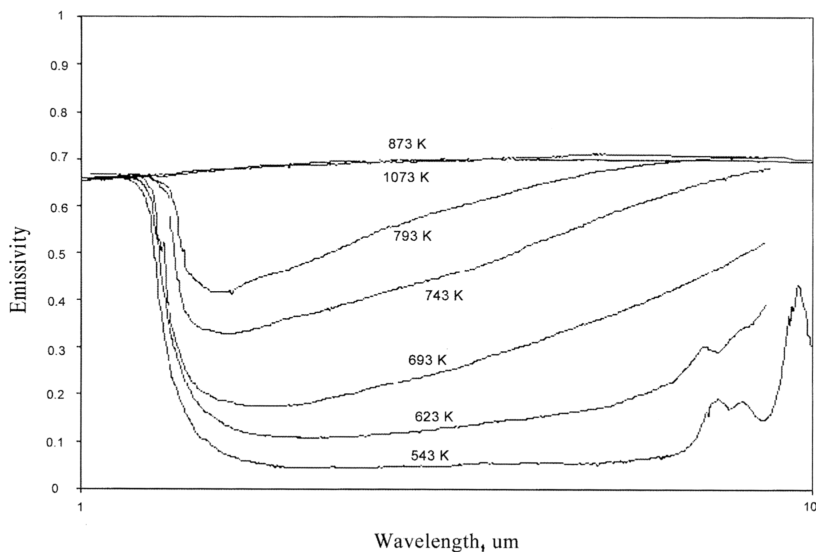

Fig. 3. Sato's [1] results redrawn to reflect changes in emissivity with wavelength in the range of 1 to 10 μm.

15 $\Omega \cdot$cm and thickness 1.77 mm. In Fig. 3, Sato's experimental data are plotted for the wavelength range 1 to 10 μm.

The total contribution to emissivity, $\varepsilon(\lambda, T)$, is given by

$$\varepsilon(\lambda, T)_{\text{total}} = \varepsilon(\lambda, T)_{\text{free carrier}} + \varepsilon(\lambda, T)_{\text{absorption edge}} + \varepsilon(\lambda, T)_{\text{phonon}}$$

For photon energy, $E_{\text{photon}} \geqslant E_g$, with E_g the bandgap, i.e., $\lambda_{\text{photon}} \leqslant \lambda_E$, the wavelength corresponding to the absorption edge; emissivity contributions are due to bandgap or above bandgap-absorption. For $E_{\text{photon}} < E_g$, the emissivity contributions are due to below-bandgap absorption. The free carrier absorption mechanism plays the dominant role in doped semiconductors in the short-wavelength range [10, 11]. In the long-wavelength range ($\lambda > 6$ μm), phonons contribute to emissivity changes. These properties are functions of temperature. As shown in Figs. 2 and 3, the emissivity of silicon is high in the visible region. This is due to contributions from band-to-band transitions. At low temperatures and long wavelengths ($1.2 < \lambda < 6$ μm), silicon is transparent to photons and hence the emissivity is low in this wavelength range. As the material approaches intrinsicity, the material becomes opaque and the emissivity increases due to free carrier absorption. Eventually, the emissivity of silicon becomes high and constant, almost independent of wavelength, at high temperatures, reaching a value of 0.67 at 1073 K.

4.3. Emissivity Models

The ability to predetermine temperature with reproducible accuracy is of fundamental importance in semiconductor processing. This is of utmost importance in nonequilibrium processes such as rapid thermal processing. Utilizing the spectral emissometer, we have attempted to correlate the emissivity of silicon with the wavelength and temperature using empirical methods [12]. Hebb and Jensen [13] have proposed a semiempirical model known as the Multirad based on the matrix method of Abeles [14]. This model assumes that the layers are optically smooth and parallel. In addition, the materials are assumed to be optically isotropic. The model facilitates calculations of the radiative properties of single-or multilayer stacks as functions of the angle of incidence, wavelength, and temperature. The advantage of the Multirad model is that it can handle spectral optical properties as well as the total absorption, reflection, and transmission. The model utilizes the Drude approximation to determine the effects of doping and temperature on the optical constants, the refractive index n, and the extinction coefficient k. A model proposed by Sopori [15], known as

PV-Optics, is the most extensive model that treats nonplanar surfaces. Besides using general optics rules, the model also utilizes the known optical constants obtained from various sources for various temperatures and doping concentrations. It does tedious calculations that resemble the Monte Carlo simulations for individual rays of light incident on planar or nonplanar surfaces.

In Fig. 4, the wavelength- and temperature-dependent emissivity of n-Si is simulated using the Multirad model. The wafer thickness and doping concentration correspond to those used in Sato's experimental studies. In the wavelength range 0.4 to 1 μm, the emissivity of silicon increases rapidly from 0.45 to 0.68 and decreases to 0.19 at 1.2 μm. This is almost independent of the temperature. In the temperature range 420 to 800°C, the emissivity of silicon increases from 0.19 to almost 0.7 at 5 μm. The emissivity remains constant in the 5- to 10-μm wavelength range. At temperatures > 600°C, the emissivity of silicon reaches its intrinsic value of 0.71. It may be noted here that while there are subtle differences in the raw data on the emissivity of silicon between the results of Sato and those of the simulation, in general, they are in agreement with one another.

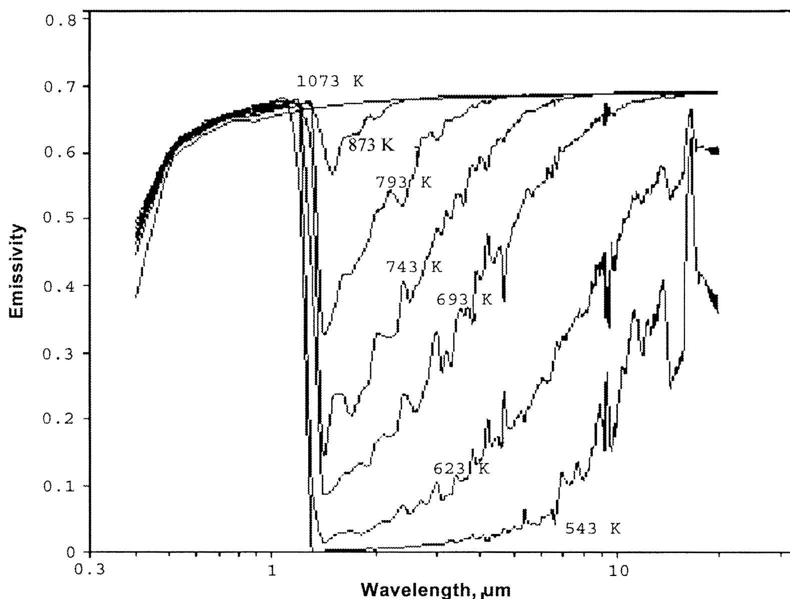

Fig. 4. Simulated emissivity results as function of wavelength for double-side polished n-Si of thickness 1770 μm and doping concentration 2.94×10^{14} cm^{-3}.

Our experimental results of emissivity measurements of single-side polished silicon, utilizing the spectral emissometer, are summarized in Fig. 5. As shown in this figure, the emissivity of silicon saturates at a value of 0.67 and remains constant in the wavelength range 2 to 10 μm. The observed sharp features in the infrared spectra in the wavelength range 1 μm (10,000 cm^{-1}) to 20 μm (500 cm^{-1}) are due to the presence of the following infrared sensitive molecules: (a) C in Si, 16.47 μm (607 cm^{-1}); (b) SiO_2, 9.01 μm (1110 cm^{-1}); (c) interstitial O_2 in Si, 8.85 μm (1130 cm^{-1}), (d) H_2O, 6.25 and 2.86 μm (1600 and 3500 cm^{-1}); (e) CO_2, 4.17 μm (2400 cm^{-1}); and (f) Si_3N_4, 8.29 μm (1206 cm^{-1}). The numbers in parentheses are the corresponding wave numbers. It should be noted here that the silicon wafer considered in this study is of the n-type, of doping concentration 1.22×10^{19} to $1.31 \text{x} 10^{18}$ cm^{-3} and thickness 400 to 457 μm. From a comparison of Fig. 5 with Fig. 2, the influence of the doping concentration and thickness on the variation in emissivity with wavelength is minimal, especially at high temperatures. However, for the heavily doped silicon wafers considered in our study, the absolute value of emissivity exceeds 0.67. The simulation of emissivity of this heavily doped silicon wafer in Fig. 6, using

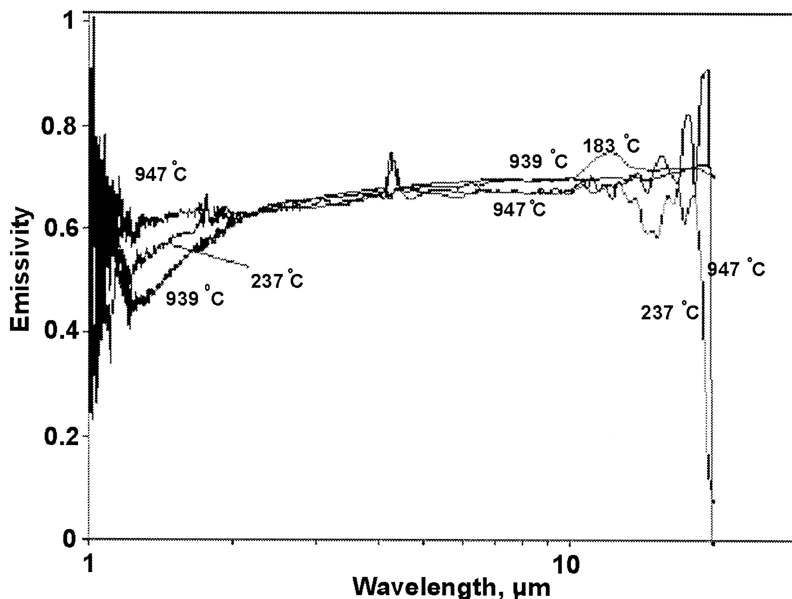

Fig. 5. Experimental results of emissivity as function of wavelength for single-side polished n-Si of thickness 400 to 457 μm and doping concentration 1.22×10^{19} to 1.31×10^{18} cm^{-3}.

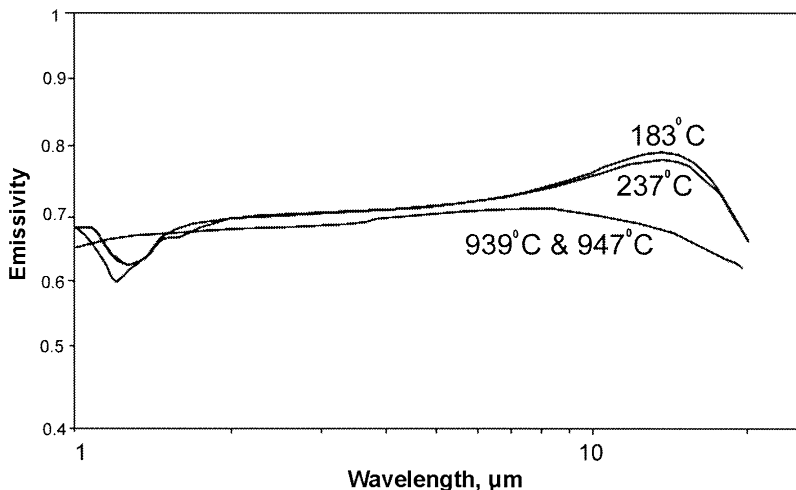

Fig. 6. Results of simulation of emissivity as function of wavelength for single-side polished n-Si of thickness 400 μm and doping concentration 1.22×10^{19} cm^{-3}.

Multirad, shows results similar to those in Fig. 5. It may be noted here that the optical properties of heavily doped silicon are still largely unavailable [16] in the literature.

4.4. Choice of Wavelengths for Pyrometry in RTP

In the silicon semiconductor industry, most of the manufacturers of commercial RTP systems have chosen pyrometers to operate at certain specific wavelengths [17]. In recent years, leading RTP equipment manufacturers, such as Applied Materials and Steag-AST, have chosen a two-wavelength approach, one close to the absorption edge of silicon and the other in the near-mid IR range. In Tables I–IV, we have summarized the simulated values of emissivity of silicon as functions of doping type, temperature, and wavelength. The thickness of the wafer considered in these simulations has been kept constant at 700 μm—a value representative of today's 150- or 200-mm-diameter wafers. Also included in the tables are values of emissivity corresponding to 10.6 μm—a wavelength of interest in the phonon range. With recent advancements in spike anneals and extremely short-time anneals [18], the significance of studies such as the temperature-dependent emissivity becomes questionable. This is because of the extremely short durations associated with such fast-ramp processes and the comparatively long time constants associated with control systems that are based on pyrometers and/or thermocouples.

Table I. Results of Simulations of Emissivity as a Function of Temperature for Wavelengths of Interest for Pyrometry (Doping Concentration, of 10^{17} cm^{-3} for n-Si and p-Si; Thickness, 700 μm)

Temp.	30°C		200°C		500°C		700°C		1000°C	
λ(μm)	n-Si	p-Si	n-Si	p-Si	n-Si	p-Si	n-Si	p-Si	n-Si	p-Si
0.8	0.672	0.672	0.667	0.667	0.657	0.657	0.651	0.651	0.643	0.643
0.9	0.677	0.677	0.673	0.673	0.661	0.661	0.651	0.651	0.635	0.635
1	0.681	0.681	0.678	0.678	0.667	0.667	0.658	0.658	0.644	0.644
1.1	0.282	0.28	0.649	0.649	0.671	0.671	0.663	0.663	0.65	0.65
2.4	0.051	0.076	0.104	0.137	0.385	0.385	0.68	0.68	0.677	0.677
2.7	0.068	0.099	0.116	0.148	0.441	0.441	0.682	0.682	0.679	0.679
3.4	0.08	0.116	0.105	0.141	0.518	0.518	0.684	0.684	0.684	0.684
4.5	0.179	0.24	0.244	0.289	0.61	0.61	0.685	0.685	0.689	0.689
10.6	0.548	0.582	0.602	0.602	0.689	0.689	0.689	0.688	0.692	0.692

4.5. Wafer in an RTP Chamber

RTP systems have evolved considerably since their inception. The most common approach to process a wafer in the RTP chamber is to heat the wafer from the top, with the polished side facing the pyrometer and the lamps. In Fig. 7, a schematic of the possible configurations of a wafer in the RTP chamber is shown. Figure 7b represents the flipped situation of

Table II. Results of Simulations of Emissivity as a Function of Temperature for Wavelengths of Interest for Pyrometry (Doping Concentration, 10^{18} cm^{-3} for n-Si and p-Si; Thickness, 700 μm)

Temp.	30°C		200°C		500°C		700°C		1000°C	
λ(μm)	n-Si	p-Si	n-Si	p-Si	n-Si	p-Si	n-Si	p-Si	n-Si	p-Si
0.8	0.672	0.672	0.667	0.677	0.657	0.657	0.651	0.651	0.643	0.643
0.9	0.678	0.677	0.673	0.673	0.661	0.661	0.651	0.651	0.635	0.635
1	0.68	0.68	0.678	0.678	0.667	0.667	0.658	0.658	0.644	0.644
1.1	0.326	0.355	0.653	0.659	0.672	0.672	0.664	0.663	0.65	0.65
2.4	0.536	0.518	0.456	0.578	0.635	0.637	0.681	0.681	0.677	0.677
2.7	0.572	0.574	0.548	0.593	0.657	0.667	0.683	0.682	0.68	0.68
3.4	0.632	0.67	0.589	0.665	0.683	0.682	0.684	0.684	0.681	0.684
4.5	0.689	0.691	0.681	0.689	0.689	0.689	0.686	0.685	0.69	0.69
10.6	0.706	0.703	0.702	0.699	0.694	0.691	0.691	0.689	0.692	0.692

Table III. Results of Simulations of Emissivity as a Function of Temperature for Wavelengths of Interest for Pyrometry (Doping Concentration, 10^{19} cm^{-3} for n-Si and p-Si; Thickness, 700 μm)

Temp.	30°C		200°C		500°C		700°C		1000°C	
λ(μm)	n-Si	p-Si	n-Si	p-Si	n-Si	p-Si	n-Si	p-Si	n-Si	p-Si
0.8	0.672	0.672	0.667	0.667	0.658	0.657	0.651	0.651	0.643	0.643
0.9	0.678	0.678	0.673	0.673	0.661	0.661	0.652	0.652	0.635	0.635
1	0.683	0.683	0.678	0.678	0.668	0.667	0.659	0.659	0.644	0.644
1.1	0.684	0.679	0.678	0.679	0.672	0.672	0.664	0.644	0.651	0.651
2.4	0.701	0.7	0.697	0.696	0.689	0.688	0.684	0.683	0.68	0.679
2.7	0.702	0.701	0.699	0.697	0.691	0.69	0.686	0.684	0.683	0.681
3.4	0.705	0.703	0.702	0.7	0.694	0.692	0.689	0.687	0.688	0.686
4.5	0.71	0.706	0.707	0.703	0.699	0.695	0.694	0.69	0.696	0.693
10.6	0.731	0.718	0.754	0.723	0.725	0.704	0.711	0.697	0.689	0.689

Fig. 7a, with the rough side of the wafer facing the lamps. Surface roughness leads to light trapping, resulting in increased emissivities [19, 20] in silicon. An ideal solution, especially for low-temperature processing, must incorporate pyrometers on the back side of the wafer as shown in Fig. 7c. Since silicon is transparent at low temperatures, the pyrometers on the back side should incorporate a wavelength correction for the lamps. This approach will also assist in correcting for environmental variations in the process chamber and possible growth of layers on the wafer back side.

Table IV. Results of Simulations of Emissivity as a Function of Temperature for Wavelengths of Interest for Pyrometry (Doping Concentration, 10^{20} cm^{-3} for n-Si and p-Si; Thickness, 700 μm)

Temp.	30°C		200°C		500°C		700°C		1000°C	
λ(μm)	n-Si	p-Si	n-Si	p-Si	n-Si	p-Si	n-Si	p-Si	n-Si	p-Si
0.8	0.675	0.674	0.67	0.669	0.66	0.659	0.654	0.653	0.645	0.644
0.9	0.681	0.68	0.677	0.675	0.665	0.664	0.655	0.654	0.638	0.637
1	0.687	0.686	0.683	0.681	0.672	0.67	0.663	0.662	0.648	0.647
1.1	0.692	0.69	0.688	0.686	0.677	0.676	0.669	0.667	0.656	0.654
2.4	0.728	0.717	0.728	0.717	0.718	0.707	0.711	0.7	0.704	0.693
2.7	0.735	0.722	0.739	0.724	0.728	0.713	0.72	0.705	0.712	0.698
3.4	0.752	0.731	0.769	0.742	0.754	0.727	0.743	0.717	0.731	0.709
4.5	0.765	0.741	0.84	0.777	0.803	0.748	0.777	0.731	0.745	0.717
10.6	0.505	0.626	0.2	0.444	0.334	0.565	0.411	0.601	0.545	0.582

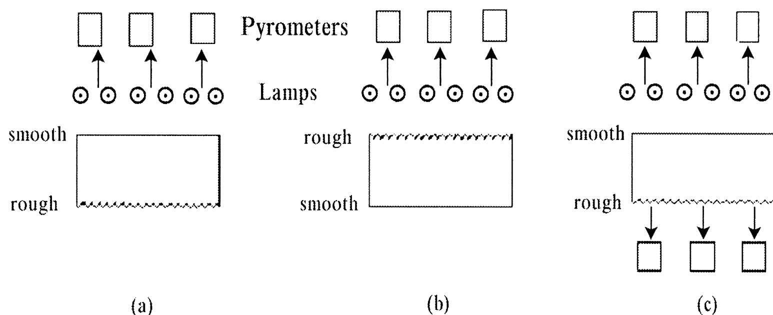

Fig. 7. Schematic of process configuration of a single-side polished Si wafer in an RTP system. (a) Typical configuration of a silicon wafer in an RTP chamber; (b) flipped case of a; (c) proposed scheme of pyrometry for low-temperature processing.

To understand the influence of surface roughness on the radiative properties of silicon, we investigated the temperature-dependent optical properties of silicon using the spectral emissometer. The results of this study are presented in Figs. 8 and 9. In Fig. 8, the transmittance and reflectance, as measured from the front and back sides of the same wafer, are compared for three representative temperatures. From these figures, the major effect on the emissivities is seen to be from the change in transmittance for the given sample for the incidence on the polished side versus the incidence on the rough side. In Fig. 9, the emissivity as measured from the front polished side and the back rough side on the same silicon wafer as a function of wave number at the same specific temperatures is shown. As shown in these figures, the emissivity of the rough side is higher than that of the polished side. This remains the case until the sample becomes opaque to subbandgap radiation at temperatures above 700°C. The approach proposed in Fig. 7c is based on the observation in Figs. 8 and 9.

4.6. Influence of Coatings

Coatings can have tremendous impact on the ability to predict temperature distribution across a wafer during processing. It is therefore critical to understand the changes in emissivity with wavelength and temperature. In Fig. 10, our experimental results on the emissivity of 63.5-nm-thick SiO_2/Si, as a function of temperature, are presented. Because of their low extinction coefficients, dielectrics such as SiO_2 are media of low losses. Thus, light reflected at the SiO_2/Si interface can constructively or destructively interfere with the light reflected at the top surface, especially if there is a high degree of coherency when the oxide thickness is comparable to the

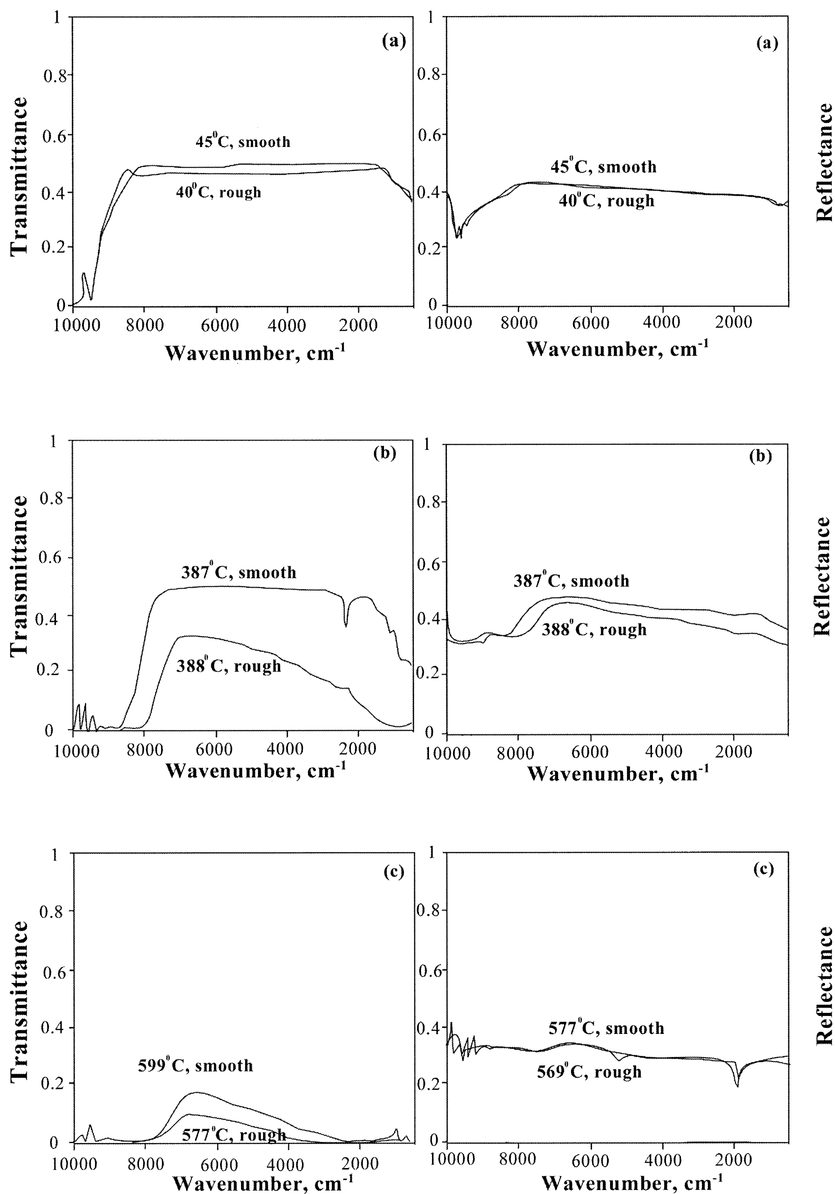

Fig. 8. Experimental transmittance and reflectance of Si as a function of wave number for three temperatures: (a) 45°C, smooth; 40°C, rough; (b) 387°C, smooth; 388°C, rough; (c) 599°C, smooth; 577°C, rough.

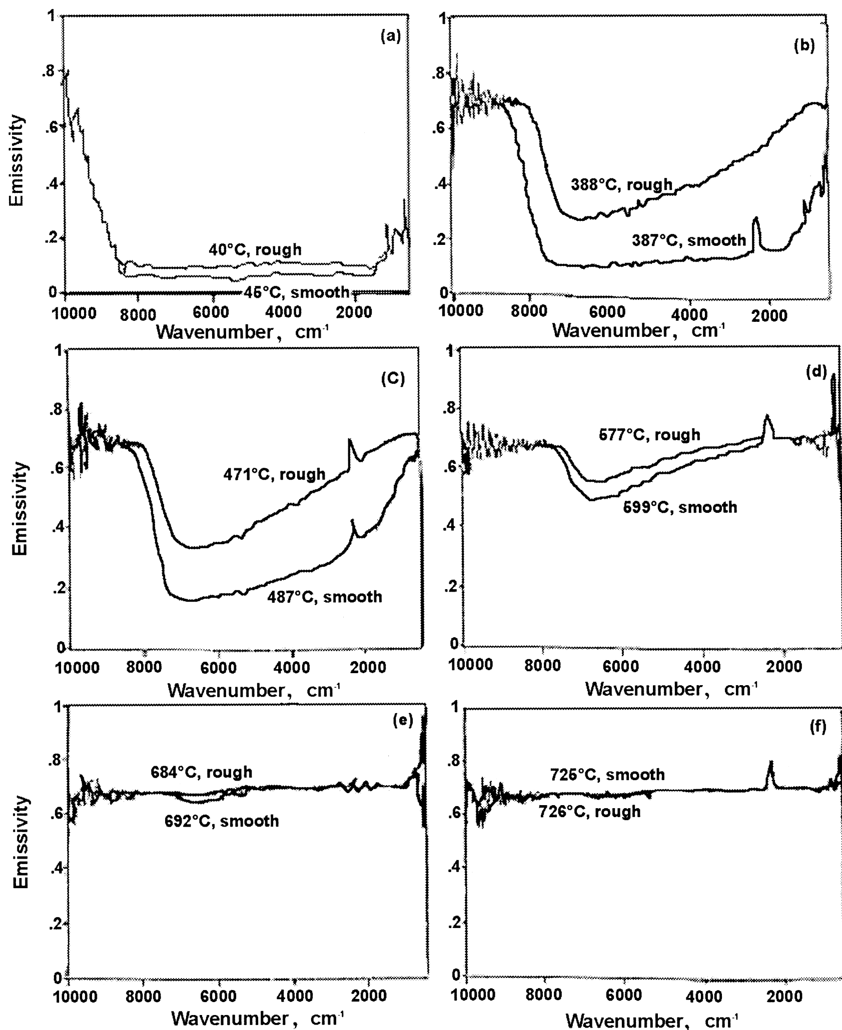

Fig. 9. Experimental emissivity versus wave number of single-side polished n-Si at selected temperatures.

wavelength of the incident light. The absorption coefficient of SiO_2 has a very weak dependence on temperature. The interference effect will be the dominant factor influencing the apparent reflectance of the wafer. Thus, if the interference of the two reflected waves, one from the top and the other from the bottom planes of the oxide, is constructive, the measured reflectance will be a maximum resulting in minimum emissivity, and the opposite

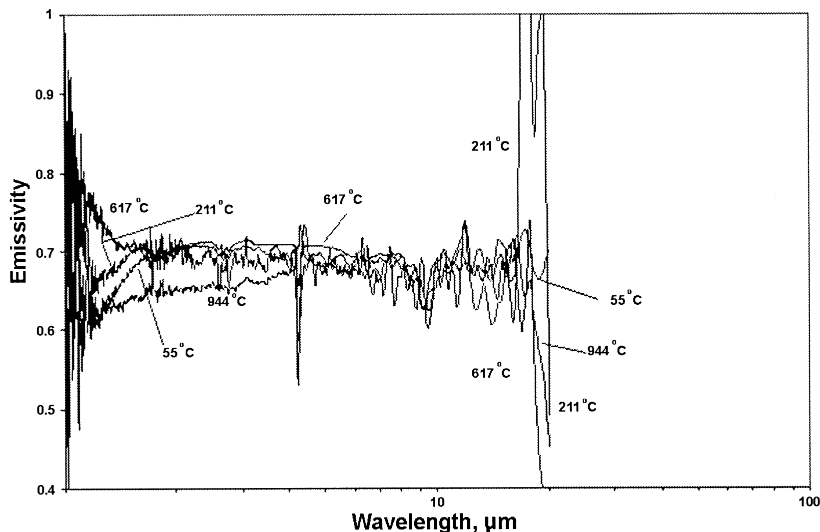

Fig. 10. Experimental results on emissivity of 65.3-nm SiO_2 on 700-μm n-Si of doping concentration 10^{18} cm^{-3} as a function of wavelength (SiO_2/Si).

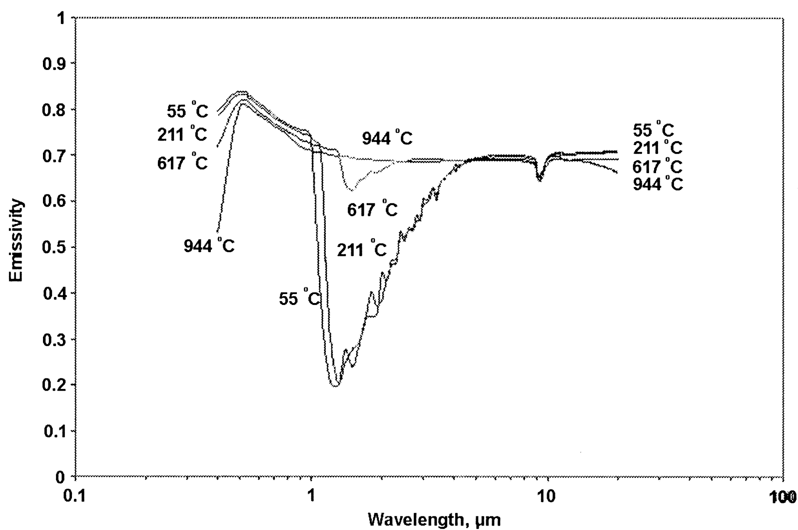

Fig. 11. Simulated results on emissivity of 65-nm SiO_2 on 700-μm n-Si of doping concentration 10^{18} cm^{-3} as a function of wavelength (SiO_2/Si).

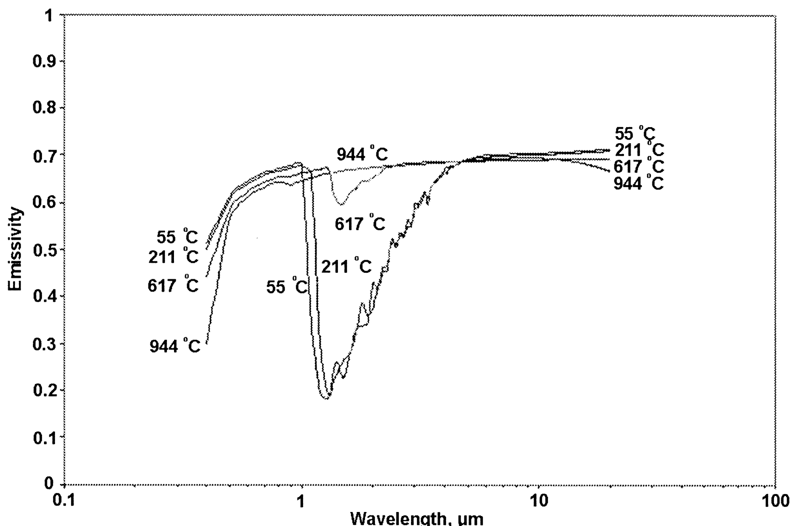

Fig. 12. Simulated results on emissivity of 700-μm n-Si on 65-nm SiO_2 of doping concentration 10^{18} cm^{-3} as a function of wavelength (Si/SiO_2).

is true. The measured emissivity in Fig. 10 does not reflect this behavior. The thickness of the SiO_2 is very small compared with the wavelength of photons. However, it is to be noted that the experimental data are also noisy because of the deployment of the oxyacetylene torch to heat the wafer. The results of the simulation of emissivity of this wafer, using Multirad, are presented in Fig. 11. At high temperatures, the emissivity of SiO_2/Si approaches that of silicon. The feature near 9 μm is due to SiO_2. To demonstrate the effect of flipping the wafer on emissivity, we have considered the simulation of emissivity of Si/SiO_2 with the same material specifications. The results of this simulation are presented in Fig. 12. A comparison of the results in Fig. 12 with those in Fig. 11 shows significant differences in the emissivity in the short-wavelength region. In the infrared range of wavelengths, the significant difference is the absence of the SiO_2 signature at 9 μm. At high temperatures, silicon becomes opaque, and therefore, the influence of coatings, surface roughness, and doping on the emissivity of silicon becomes negligible.

5. CONCLUSIONS

An investigation of the emissivity of silicon-related material has been presented. Necessary corrections have been proposed to comprehend the

celebrated work of Sato. A spectral emissometer, capable of simultaneous measurement of reflectance, transmittance, emittance, and temperature, operating in the wavelength range 1 to 20 μm, has been utilized to examine the radiative properties of silicon-related materials. Simulations of the wavelength and temperature dependent emissivity of these materials have been performed using Multirad. The experimentally measured emissivities are seen to be generally in accord with simulations.

ACKNOWLEDGMENTS

This work has been partially supported in various stages by grants from DARPA, DOD, SEMATECH, and the U.S. Department of Energy.

REFERENCES

1. K. Sato, *Jpn. J. Appl. Phys.* **6**:339 (1967).
2. J. Hebb and K. F. Jensen, *"Multi-Rad" User's Manual* (SEMATECH, Austin, Texas, 1997).
3. N. M. Ravindra, S. Abedrabbo, W. Chen, F. M. Tong, A. K. Nanda, and A. C. Speranza, *IEEE Trans. Semicond. Manuf.* **11**:30 (1998).
4. N. M. Ravindra, S. Abedrabbo, O. H. Gokce, F. M. Tong, A. Patel, R. Velagapudi, G. D. Williamson and W. P. Maszara, *IEEE Trans. Comp. Pack. Technol.* **21**:441 (1998).
5. S. Abedrabbo, F. M. Tong, N. M. Ravindra, J. Gelpey, S. Marcus, and A. T. Fiory, *J. Electron. Mater.* **27**:1323 (1998).
6. S. Abedrabbo, J. C. Hensel, A. T. Fiory, and N. M. Ravindra, *J. Electron. Mater.* **28**:1390 (1999).
7. M. Born and E. Wolf, *Principles of Optics*, 4th ed. (Pergamon Press, New York, 1970), p. 381.
8. N. M. Ravindra, O. H. Gokce, F. M. Tong, S. Abedrabbo, V. Rajasekhar, A. Patel, G. Williamson, W. Maszara, A. Nanda, and T. Speranza, in *Proceedings 3rd International Workshop on Thermal Investigations of ICs and Microstructures* (Institute of Electrical and Electronics Engineers, Cannes, France, 1997), p. 40.
9. J. R. Markham, K. Kinsella, R. M. Carangelo, C. B. Brouillitte, M. D. Carangelo, P. E. Best, and P. R. Solomon, *Rev. Sci. Instrum.* **64**:2515 (1993).
10. N. M. Ravindra, W. Chen, F. M. Tong, and A. Nanda, in *Transient Thermal Processing Techniques*, N. M. Ravindra and R. K. Singh, eds. (TMS—The Minerals Metals Materials Society, Warrendale, PA, 1996), p. 159.
11. N. M. Ravindra, F. M. Tong, S. Abedrabbo, W. Chen. W. Schmidt, A. Nanda, T. Speranza, and A. M. Tello, in *Proceedings Fourth International Conference on Rapid Thermal Processing*, Boise, ID (1996), p. 190.
12. N. M. Ravindra, F. M. Tong, W. F. Kosonocky, J. R. Markham, S. Liu, and K. Kinsella, in *Proceedings Materials Research Society, Rapid Thermal and Integrated Processing III, Vol. 342* (1994), p. 431.
13. J. P. Hebb and K. F. Jensen, *J. Electrochem. Soc.*, **143**:1142 (1996).
14. F. Abeles, *Ann. Phys.* **5**:596 (1950).
15. B. Sopori, W. Chen, J. Madjdpour, and N. M. Ravindra, *J. Electron. Mater.* **28**:1385 (1999).

16. P. J. Timans, in *Proceedings, Materials Research Society, Rapid Thermal and Integrated Processing V, Vol. 429* (1996), p. 3.
17. S. Abedrabbo, N. M. Ravindra, W. Chen, V. Rajasekhar, O. H. Gokce, A. T. Fiory, B. Nguyenphu, A. Nanda, T. Speranza, W. Maszara, and G. Williamson, in *Proceedings, Materials Research Society, Rapid Thermal and Integrated Processing VI, Vol. 470* (1997), p. 69.
18. A. Agarwal, H. J. Gossmann, and A. T. Fiory, *J. Electron. Mater.* **28**:1333 (1999).
19. S. Abedrabbo, J. C. Hensel, O. H. Gokce, F. M. Tong, B. Sopori, A. T. Fiory, and N. M. Ravindra, in *Proceedings, Materials Research Society, Rapid Thermal and Integrated Processing VII, Vol. 525* (1998), p. 95.
20. S. Abedrabbo, J. C. Hensel, A. T. Fiory, B. Sopori, W. Chen, and N. M. Ravindra, *Mater. Sci. Semicond. Process.* **1**:187 (1998).